frontiers | Frontiers in Earth Science

TYPE Original Research
PUBLISHED 20 October 2023
DOI 10.3389/feart.2023.1255813

OPEN ACCESS

EDITED BY
Jie Liao,
Sun Yat-sen University, China

REVIEWED BY
Lianghui Guo,
China University of Geosciences, China
Zhongtai He,
China Earthquake Administration, China
Gaofeng Ye,
China University of Geosciences, China

*CORRESPONDENCE
Xiaosong Xiong,
benxung@126.com

RECEIVED 09 July 2023
ACCEPTED 03 October 2023
PUBLISHED 20 October 2023

CITATION
Wang Z, Xiong X, Wu G, Li Z, Ye Z and Jin Z (2023), Crustal structure and deformation mechanism of the western northeast Tibetan Plateau.
Front. Earth Sci. 11:1255813.
doi: 10.3389/feart.2023.1255813

Crustal structure and deformation mechanism of the western northeast Tibetan Plateau

Zining Wang, Xiaosong Xiong*, Guowei Wu, Zhichao Li, Zhuo Ye and Zhongyuan Jin

Chinese Academy of Geological Sciences, Beijing, China

The collision between the Indian and Eurasian plates continues to drive significant deformation and uplift within the interior of the Tibetan Plateau, together with its outward expansion along the margins. In particular, the North Qilian Shan fold-thrust belt (NQLS) and the Hexi Corridor basins (HXBS) represent the northernmost region of the northeastern Tibetan Plateau. This area serves as a natural laboratory for deciphering mechanisms of crustal deformation and thickening along the plateau's margins. Specifically, the northeastern Tibetan Plateau has been attributed to 1) southward underthrusting of the Asian lithosphere, 2) distributed shortening and crustal thickening, 3) vertical inflation of the Tibetan crust due to mid-lower crustal channel flow, and 4) intracontinental subduction facilitated by large-scale strike–slip faults. The exact mechanism underlying the most concentrated convergent stress in the western segment of NQLS–HXBS remains a subject of debate. To address this uncertainty, we gathered seismic data along a 130-km-long linear array that extends northward from NQLS, traversing the Jiuquan Basin and reaching the Huahai Basin. Our analysis, conducted through the receiver function method, reveals intriguing findings. The Moho depth deepens from 45–50 km beneath the Huahai Basin to 55–60 km beneath NQLS. Notably, a double Moho structure emerged, marked by a distinctive near-flat positive amplitude at a depth of 45–50 km beneath NQLS within a distance of 0–50 km. Our study presents a comprehensive analysis of the crust-scale deformation mechanism, shedding light on the following key aspects: 1) the development of a decollement at 12–20 km depth decoupling the upper and lower crust; 2) deformation of the upper crust occurring through south-dipping brittle thrust faults, while the lower crust features imbricate structures and duplexes; 3) evidence pointing to the underthrusting of the Beishan Block beneath NQLS, indicated by the double Moho beneath NQLS; and 4) the formation of a Moho ramp beneath the Jiuquan Basin, facilitating the transfer of shortening stress from beneath NQLS and HXBS to the north. In the context of the western segment of NQLS and HXBS, our speculation is that coupled distributed shortening and Beishan Block subduction beneath NQLS work in tandem to accommodate crustal deformation.

KEYWORDS

Qilian Shan fold-thrust belt, northern Tibetan Plateau, Jiuquan Basin, receiver function, crustal deformation, double Moho

1 Introduction

The collision and continued convergence of the Indian and Eurasian plates since ca. 55 Ma have resulted in substantial deformation and uplift within the interior of the Tibetan Plateau, together with the outward expansion of the plateau along its margins (e.g., Molnar and Tapponnier, 1975; Tapponnier et al., 2001; Yin, 2000; Yin, 2010; ; Zhao et al., 2010; Zuza et al., 2018; Xiong et al., 2022). This collision has significantly impacted both the topography and climate of the surrounding regions (Zhang et al., 2004). However, the precise manner in which the Tibetan crust accommodates the convergence of the Indian and Eurasian plates, leading to the development of the Tibetan Plateau, remains a subject of intense debate (e.g., Cheng et al., 2019; Clark and Royden, 2000; Yin and Harrison, 2000; Tapponnier et al., 2001; van Hinsbergen et al., 2011; van Hinsbergen et al., 2012; Yakovlev and Clark, 2014; Ingalls and Stedman, 2016; Zuza et al., 2016; Zheng et al., 2017). Moreover, different segments of the Tibetan Plateau margins may exhibit varying deformation mechanisms, particularly across the northeastern Tibetan Plateau margin that stretches across strike for >1,000 km. (Lin et al., 2011; Duvall et al., 2013).

NQLS and the HXBS comprise the northernmost margin of the Tibetan Plateau. This contractional thrust-fold belt and foreland basin system represent an area of concentrated stress resulting from the convergence of the Indian and Eurasian plates (Xiong et al., 2019). Understanding the geometric and kinematic characteristics of the crustal structure in this region is essential for deciphering the deep interrelation between the Tibetan Plateau and the Eurasian plate. This knowledge holds the potential to significantly enhance our comprehension of continental tectonics (Yin et al., 2002; Molnar, 1988; Zhang et al., 2004; Zhou et al., 2006; Yin, 2010; Lease et al., 2012; Craddock et al., 2011; Craddock et al., 2014; Zuza et al., 2019).

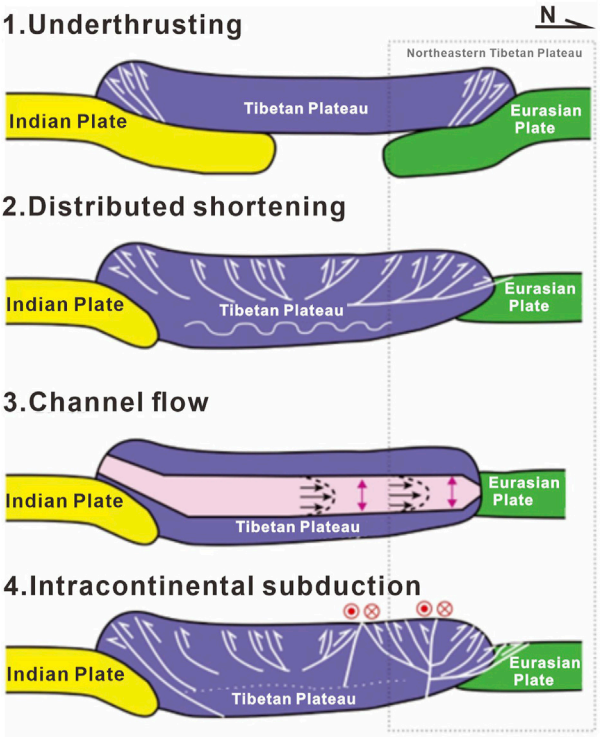

FIGURE 1
Crustal growth model map of the northeastern Tibetan Plateau (modified from Zuza et al., 2019; Wu GW. et al., 2023).

Since the 1970s (Burke and Dewey, 1973; Molnar and Tapponnier, 1975), numerous end-member models have been proposed to explain the formation of the Tibetan Plateau, as a result of intensive study (Figure 1). In the northeastern Tibetan Plateau, these models include (1) Cenozoic underthrusting of the Asian lithosphere beneath the Tibetan Plateau (Willett and Beaumont, 1994; Kind et al., 2002; Zhao et al., 2011; Feng et al., 2014; Ye et al., 2015); (2) coupled distributed crustal shortening and underthrusting of the Alxa Block beneath Tibet, accounting for the observed crustal shortening and thickness distribution (England and Houseman, 1986; Dewey et al., 1997; Huang et al., 2018; Xiong et al., 2019; Zuza et al., 2019); (3) vertical inflation of the Tibetan crust due to lateral mid-lower crustal channel flow (Zhao and Morgan, 1987; Bird, 1991; Royden et al., 1997; Clark and Royden, 2000); and (4) intracontinental subduction facilitated by large-scale strike–slip faults (Zuza et al., 2016; Wu et al., 2023b).

These tectonic models offer specific predictions regarding the location, timing of deformation, and kinematics of crustal structures in the northeastern Tibetan Plateau (Lease et al., 2012; He, 2020; Zuza et al., 2016; 2019). Therefore, crustal-scale seismic imaging can provide insights into the dominant deformation mechanism along the northern margin of the Tibetan Plateau. Despite prolific geophysical research conducted over recent decades on the northeastern Tibetan Plateau, the mechanisms driving crustal deformation remain contentious. Given that the west-to-east-trending NQLS and HXBS stretch over a span of 1,000 km, the crustal deformation mechanism may indeed vary across different segments.

In the western segment, the Moho depth is notably deeper than that in the middle-eastern Qilian Shan fold-thrust belt, with a maximum depth of 73 km beneath Hala Lake, as substantiated by studies (Cui et al., 1995; Gao et al., 1999; Jolivet et al., 2001; Huang et al., 2021). This observation supports the hypothesis that the most concentrated convergent stress is accommodated through crustal deformation in the western segment. To address this question, we gathered seismic data from a linear array spanning 130 km, extending northward from NQLS, traversing the entire Jiuquan Basin, and reaching the Huahai Basin. The data were continuously recorded over approximately 30 days using the Smart Solo IGU-16 HR 3C geophones, which are three-component geophones with a dominant frequency of 5 Hz (Figure 2B). The dense seismic array comprises 261 short-period geophones spaced at 500-m intervals. Through receiver function processing of the seismic observations, we have unveiled the crustal structure beneath the North Qilian–Huahai Basin and gained insights into the crustal deformation mechanism within the western segment of NQLS–HXBS.

2 Geological setting

The northeastern Tibetan Plateau has an average elevation of ~4.5 km, with the high topography decreasing rapidly to <1.5 km in HXBS to the north (Figure 2). Previous geophysical observations

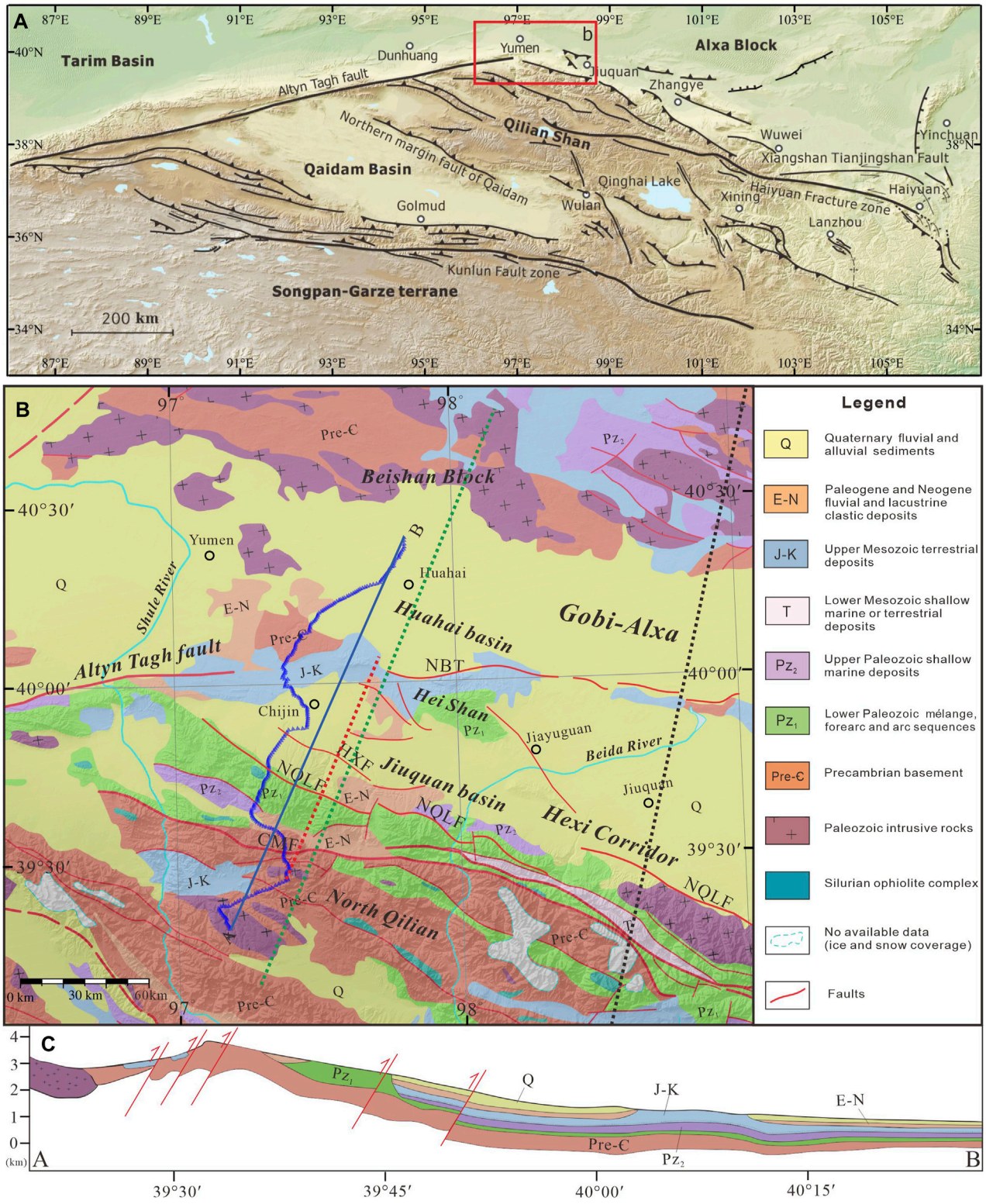

FIGURE 2
(A) Tectonic fault map of the northeastern Tibetan Plateau, including the Qilian Shan and surrounding regions (modified from Gao et al., 2013; Zuza et al., 2016). The red rectangle shows the location of Figure 2B. **(B)** Geologic map of the North Qilian Shan fold-thrust belt and the Huahai Basin (modified from Ye et al., 2021). The blue line segment represents the dense-seismic array. The red dashed line represents the CMP line. The green dashed line represents the MT line. The black dashed line represents the DSS line. **(C)** Cross section along line **(A, B)** in Figure 2B. CMF, Changma Fault; NQLF, North Qilian Fault; HXF, Hanxia Fault; NBT, North Border Thrust.

indicate that the Moho depth ranges from 55 to 73 km (Zhao et al., 2001; Yue et al., 2012; Gao et al., 2013; Yuan et al., 2013; Xu et al., 2018; Wu et al., 2023b). Additionally, the relatively stable crust beneath HXBS has a thickness of approximately 42–51 km (Cui et al., 1995; Xiong et al., 2019).

The NQLS formed as an accretionary complex due to the closure of the Qilian Ocean in the Early Paleozoic and was later reactivated following the Indian–Eurasian plate collision in the Cenozoic. The present-day tectonic belt, located between the northern Alxa Block–Beishan Block and the southern Middle Qilian Block, follows a narrow NW–SE-trending structure. This belt is truncated by the Altyn Tagh faults to the northwest (Figure 2). The Qilian Shan fold-thrust belt exhibits volcanic and magmatic rock distributions from the Paleoproterozoic to the early Paleozoic (Wu et al., 2023a). Since the Cenozoic era, NQLS has been involved in crustal thickening and deformation, marking its northernmost extension onto the Tibetan Plateau.

The Jiuquan Basin is situated at the western terminus of HXBS, and the Jiuquan Basin is bounded by the Jiayuguan fault, Altyn Tagh fault, Qilian Shan North Margin fault, and Heishan fault. Sedimentation in the Jiuquan Basin initiated in the Mesozoic, and this northwest-trending basin was subsequently influenced by the uplift of NQLS. Deep seismic reflection profiles reveal that the thickness of the Cenozoic sedimentary cover ranges between 1.5 and 2 km (Song et al., 2001; Huang et al., 2018).

The Huahai Basin lies to the north of the Jiuquan Basin bounded by the Kuantan Shan fault, Heishan fault, and Jintana Shan fault. Initially part of the Dunhuang Block, a relatively stable Precambrian block, the Huahai Basin is covered by Mesozoic–Cenozoic sediments with a sedimentary thickness of 5 km (Chen and Yang, 2010). Paleozoic granitoids have locally intruded into the sedimentary cover (refer to Figure 2).

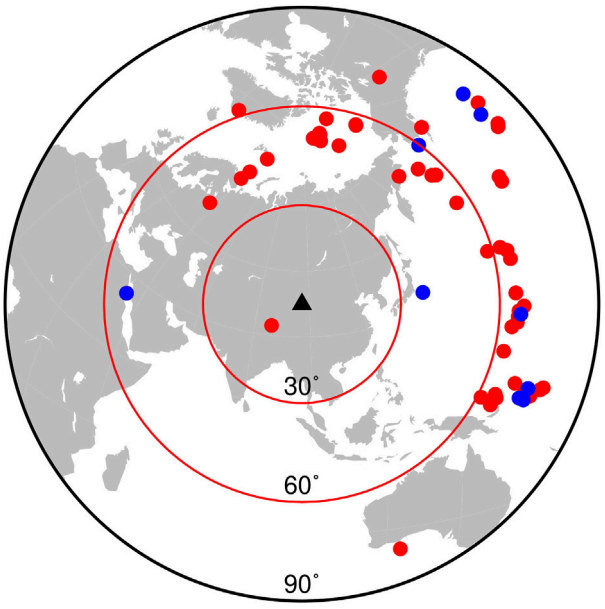

FIGURE 3
Seismic distribution map (the black triangle represents the location of the station, red circles represent the earthquake of magnitude 5–5.5, and blue circles represent the earthquake of magnitude 5.5 or above).

3 Methods and principles

In this study, we deployed a dense array of 261 Smart Solo 16 HR 3C nodal short-period seismometers for observations. These were positioned with an average spacing of 500 m in the field and operated for approximately 30 days. A receiver function is a time sequence derived from deconvolving the radial component of teleseismic P-waves. This process yields the vertical component that represents P-to-S wave conversion. Receiver function analysis is an effective approach for imaging crustal structures. By stacking multiple receiver functions with similar ray paths, the dense nodal array enhances the vertical resolution of receiver function images and boosts high-frequency signals (Langston, 1979; Xu et al., 2018; Ammon et al., 1990; Xu et al., 2020; Tian et al., 2021).

After obtaining the raw seismic data, several steps are typically followed to extract receiver functions. This process involves filtering, receiver function separation, and deconvolution. In practical research, receiver function studies usually focus on earthquakes with a magnitude of 5 or higher. For data preprocessing, earthquakes within 30°–90° epicentral distances (refer to Figure 3) were selected. We acquired a total of 47 seismic events with a magnitude (Ms) of ≥5 and epicentral distances between 30° and 90° from the IRIS website during the data acquisition period. Data for each station were extracted from 900 s after the origin time. Raw seismic data at stations contain not only information about the subsurface medium structure but also various types of noise from surface human activities, unrelated to underground structures and tectonics. Hence, noise filtering is essential, often using low-pass and band-pass filters. After removing the instrument response, the data were down-sampled from 500 Hz to 50 Hz (0.002 s–0.02 s), and band-pass filtering was conducted within the frequency range of 0.5 Hz–10 Hz. The raw three-component data coordinate system was rotated from NEZ to RTZ. Ray parameters and theoretical arrival times were computed. After rotation, P-wave energy concentrated mainly in the radial R component, while azimuthal energy in the tangential T component. Finally, time-domain deconvolution algorithm calculations were performed (Ligorria and Ammon, 1999), using a Gaussian filter factor 2. This iterative deconvolution subtracts the radial component of observed seismic records from calculated theoretical receiver functions, iteratively updating differences until either iterations exceed a threshold or differences fall within a given tolerance range (refer to Figure 4). Computed receiver functions were then selected, focusing on data with clear P-wave phases, distinct seismic phases, and good Ps–PpPs consistency.

The common midpoint (CMP) stacking concept, initially introduced by Dueker and Sheehan (1997) for reflection waves, was adapted for imaging converted waves in receiver functions. This method corrects and stacks slanting receiver functions dynamically to create a wavefield image of the interface below the array. Building on this, Zhu and Kanamori (2000) proposed the CCP stacking method for receiver functions. Based on a given velocity model, each receiver function is projected back into the spatial domain using ray paths, followed by stacking imaging in the spatial domain (Chen et al., 2022; Cheng et al., 2023). In our study, we applied the CCP stacking method to stack the processed receiver functions. The

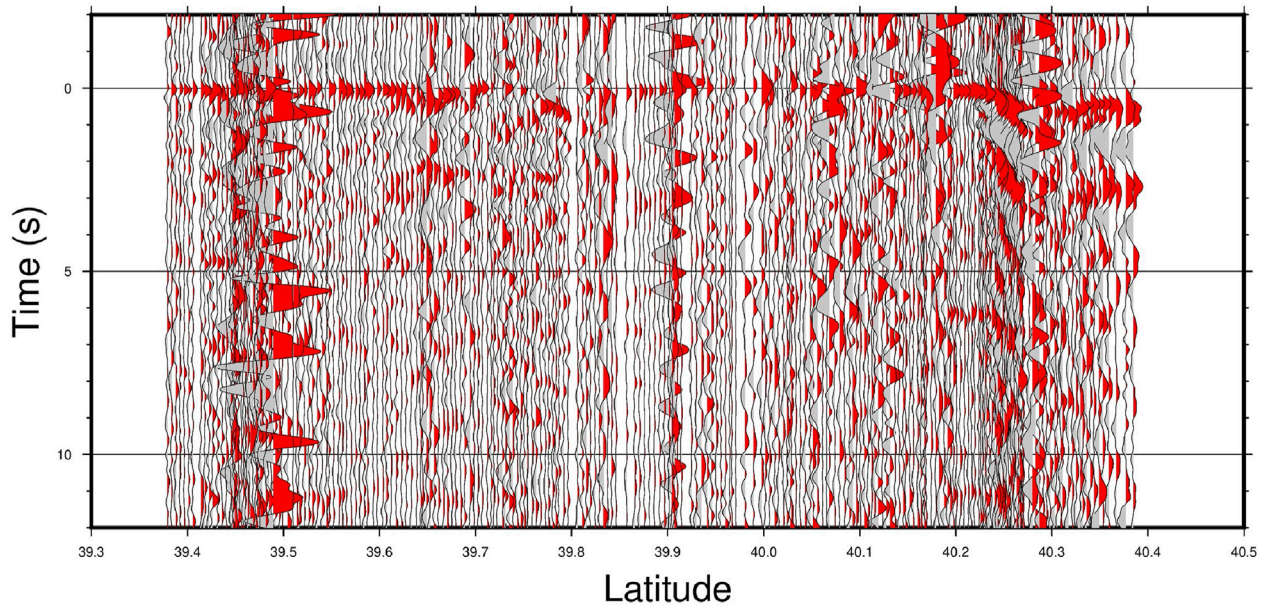

FIGURE 4
Receiver function image (receiver function of all stations in a single seismic event).

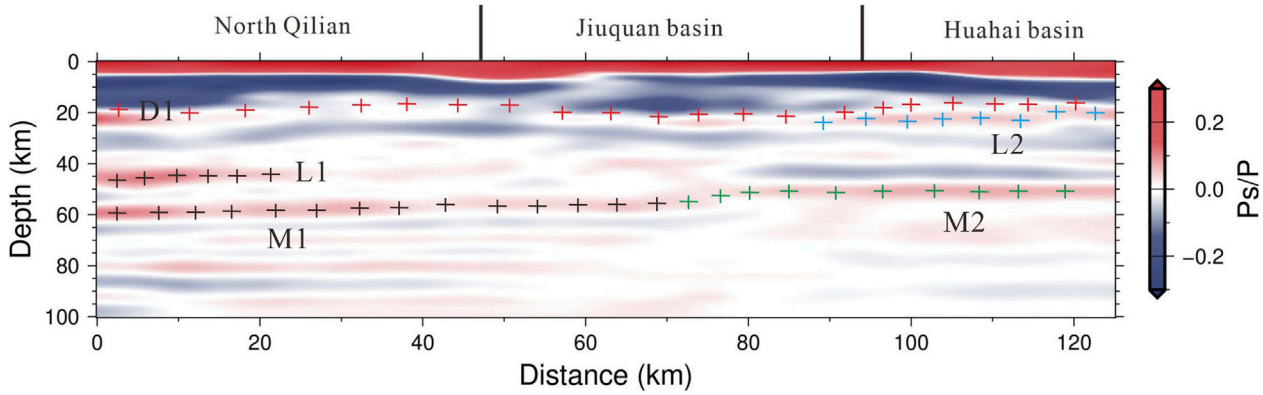

FIGURE 5
CCP superposition profile. The red colors indicate positive amplitudes (increased velocity downward); the blue colors indicate negative amplitudes (decreased velocity downward). Decollement is marked by red crosses and labeled as D1. Moho is marked by black and green crosses and labeled as L1, M1, and M2. The ductile shear zone is marked by blue crosses and labeled as L2.

method assumes a horizontally layered medium beneath the station, mapping amplitude information of processed and deconvolved receiver functions along the ray path to the conversion point. The amplitudes of receiver functions at the conversion point are stacked to obtain the medium structure below the station (refer to Figure 4).

For time–depth conversion, we utilized the reference velocity model IASP91, with a rectangular shape and a maximum depth of 100 km (Chen et al., 2022). Bins were spaced at intervals of 5 km. The time-to-depth conversion used a depth interval of 1 km, with intervals of 2 km from 0 km to 100 km. After stacking receiver functions with these settings, the CCP profile image was generated (refer to Figure 5).

4 Results

In the CCP image, red colors indicate positive amplitudes (increased velocity downward), while blue colors indicate negative amplitudes (decreased velocity downward). Our new seismic imaging reveals the following features.

A continuous positive amplitude stretches throughout the section at depths of 0–5 km; it deepens to 8 km in the contact zone of North Qilian and Jiuquan Basin and the center of the Huahai Basin; two distinct large negative amplitude bodies are visible at depths of 8–20 km below the NQLS and Jiuquan Basin; a relatively continuous positive amplitude extends at a depth of 12–20 km; the Moho, the most prominent positive velocity discontinuity, deepens

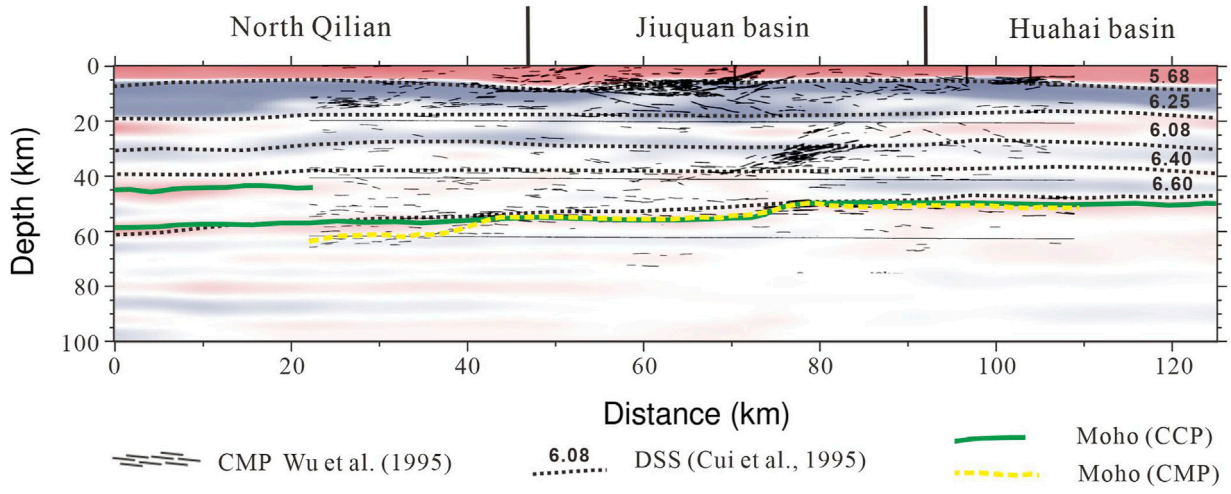

FIGURE 6
Crustal structure and Moho from different studies. Deep reflection seismic image (Wu et al., 1995) is overlain by our receiver function image (transparent) showing our interpretations of Moho and intracrustal boundaries. The CMP Moho depth is shown by the yellow line (Liu et al., 2006), and the CCP Moho depths, including the double Moho, are shown by the green dashed lines. Significant velocity boundaries are labeled with Vp (km/s) (Cui et al., 1995).

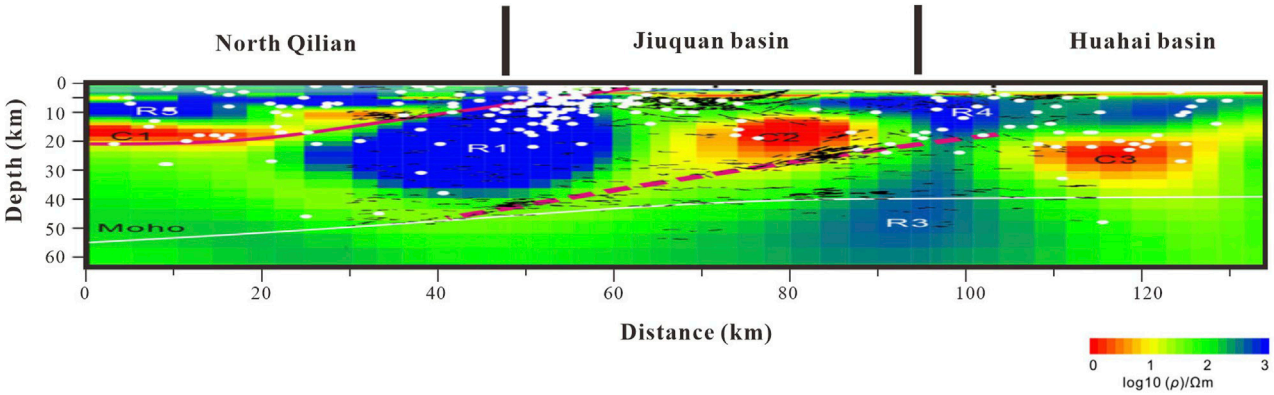

FIGURE 7
The electrical structure and deep reflection stack map (C1, C2, and C3) modified from Xiao et al. (2012) and Wu et al. (1995) are the centers of relatively low resistivity in the crust along the profile. R1, R3, R4, and R5 are the locations along the high-resistivity body at different temperatures. The red solid line represents the fault, and the red dotted line represents the boundary between the Hexi Corridor and its north. The short black line shows the seismic reflection mentioned in Wu et al. (1995) on the resistivity image. The white solid circles show the seismic activities from 1980 to 2008.

from 45–50 km beneath the Huahai Basin to 55–60 km beneath NQLS; above the bottom Moho, a distinct positive amplitude at a depth of 45–50 km beneath NQLS, within 0–50 km distance, may represent the original Moho of the marginal NQLS (Figure 5).

5 Discussion

5.1 Crustal structures

The dense stations along our profile provide high-resolution images, revealing clear and strong crustal deformations from NQLS across the Jiuquan Basin to the Huahai Basin. At a depth of 20 km along the entire section, D1 is captured, exhibiting a subtle increase beneath NQLS (Figure 5). The Golmud–Ejinaqi DSS profile showed a relatively lower velocity zone at a depth of 20 km with a P-wave velocity of 5.9 km/s compared to the surrounding 6.1 km/s P-wave velocity (Cui et al., 1995). The Diaodaban–Huahai basin deep seismic reflection profile revealed a strong reflector at the depth of 3.5–4 s TWT (approximately 12 km), which could indicate the intracrustal decollement (Wu et al., 1995; Cui et al., 1995). These data consistently suggest that D1 is the main decollement in the crust, separating it into upper and lower parts. By projecting earthquakes from 1900 to 2023 located within 100 km of our profile (Figure 8) onto the seismic section, we found that seismic activities mostly occurred above 20 km depth. A cluster of

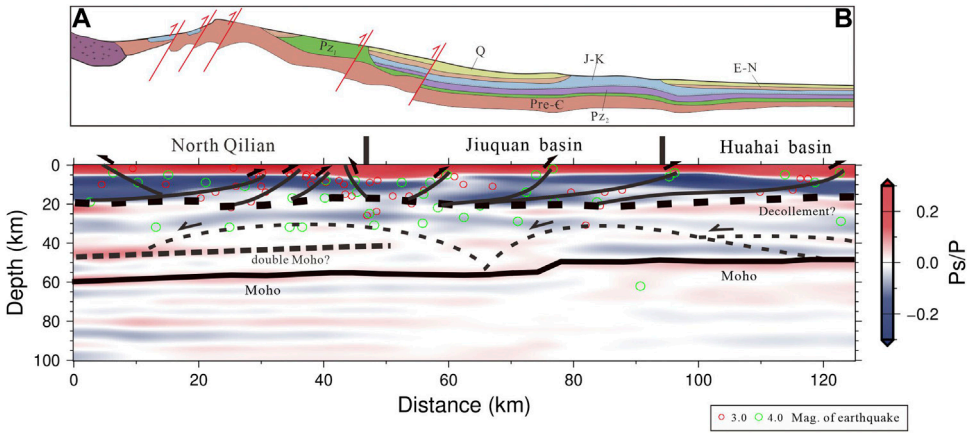

FIGURE 8
The upper image is the geological section, corresponding to Panel **(C)** in Figure 2. And the lower image is the crustal profile of local seismic superposition (the fine lines with the arrow are the ductile shear zone, and the arrows are the extension direction of the ductile shear zone. The fine dashed lines are the brittle thrust faults in the upper crust; the fine solid lines are the imbricate structures and duplexes in the lower crust. The bold dashed line represents the decollement. The Moho and the double Moho have been marked in the figure).

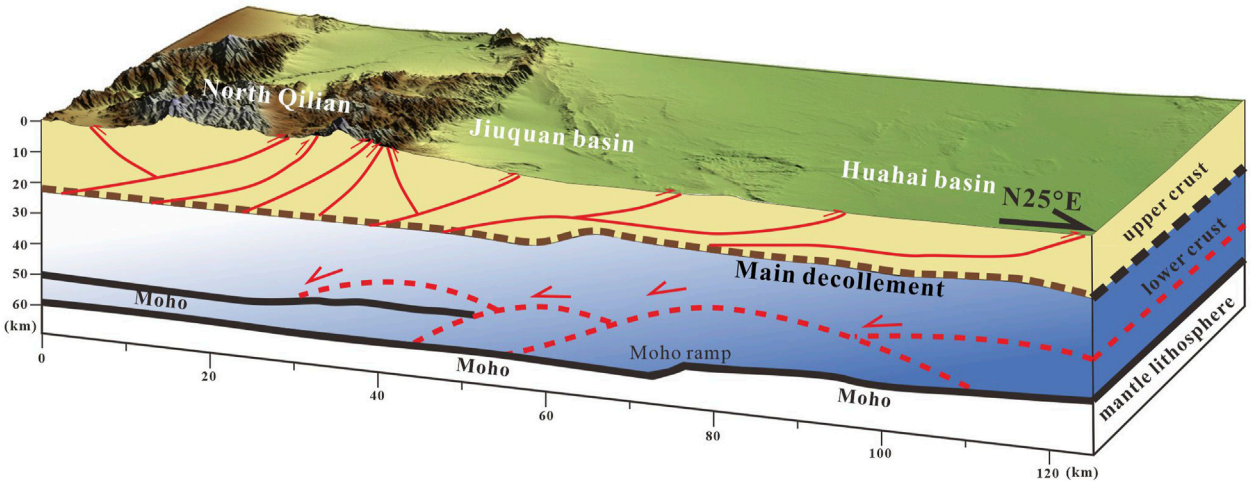

FIGURE 9
Sketch of the crustal deformation patterns across the North Qilian Shan fold-thrust belt and Huahai Basin. In the cross section, bold black lines are crustal interfaces and Moho constrained by CCP stacking; dashed lines mark decollement; red lines are the brittle thrust faults in the upper crust; red dashed lines are the imbricate structures and duplexes in the lower crust; and Moho ramp is marked in the lower crust.

earthquakes was distributed along the decollement, in alignment with geophysical observations. A continuous L1 is present at a depth of 50 km beneath the North Qilian and southern Jiuquan Basin, forming a lateral-stretching wedge with M1 below (Figure 5). Below the northern Jiuquan and Huahai basins, a near-flat M2 is distinct at depths of 45–50 km, abruptly deepening to 60 km (M1) beneath the middle Jiuquan Basin. We interpret M1 and L1 to signify a double Moho beneath NQLS, formed by the underthrusting of the North Block beneath NQLS. This double Moho was also observed in the Eastern Qilian Shan fold-thrust belt (Ye et al., 2015), representing the underthrusting of the Alxa Block beneath the Eastern Qilian Shan fold-thrust belt. In other global orogenic belts, a double Moho was detected through passive- or active-source seismic methods in West Kunlun, China, and the northern and western margins of the Yilgarn Craton, Australia (Kao et al., 2001; Kennett and Saygin, 2015). L2, preserved above M2 in the northern Jiuquan and Huahai basins, may indicate a ductile shear zone accommodating deformation in the lower crust (Figure 5).

The electrical structure of the crust shown in the MT profile (Figure 7; Xiao et al., 2012) reveals higher resistivity in NQLS compared to HXBS and beneath the Huahai Basin. The MT data display higher resistivity beneath the Huahai Basin, similar to the characteristics beneath NQLS. Three areas with lower resistivity beneath the basin, labeled C1, C2, and C3, align with the CCP image. However, the CCP image's alignment with seismic activities is more pronounced.

To the east of our study area, a deep reflection seismic profile and a 1200-km-long deep seismic sounding were previously acquired (Cui et al., 1995; Gao et al., 1999). Comparing the crustal structures of our seismic imaging with the two active-source seismic profiles along the NNE–SSW-trending survey line (Figure 6), we find that the main crustal interferences and features are relatively consistent, further validating our observations.

5.2 Implication to the crustal deformation mechanism

Extensive research on the Qilian Shan fold-thrust belt and HXBS regarding their development, evolution, and outward expansion within the northern Tibetan Plateau has been conducted using active- and passive-source seismic observations and MT soundings (Gao et al., 2001; Xiao et al., 2012; Ye et al., 2015; Shen et al., 2020; Huang et al., 2021; Sun et al., 2021; Ye et al., 2021). Different observations have led to various proposed deformation mechanism models, yet the debate persists. Our recent seismic imaging provides evidence supporting a combination of underthrusting and decoupled crustal shortening mechanisms in the western NQLS and Jiuquan Basin.

The discovery of a double Moho (L1 and M1) in the western Qilian Shan fold-thrust belt, a characteristic geodynamic feature of underthrusting globally (Zhao et al., 1993; Kao et al., 2001; Ye et al., 2015; Xu et al., 2019), suggests the southward underthrusting of the Beishan Block–Alxa Block beneath the Qilian Shan fold-thrust belt. This underthrusting might extend at least as far as NQLS. This phenomenon has been substantiated by the electrical structure and other seismic findings (Figure 7; Gao et al., 2001; Xiao et al., 2012; Huang et al., 2021; Ye et al., 2021). Recent geophysical data increasingly confirm the stable and rigid nature of the Beishan Block, which could potentially underthrust beneath more active units. The slow-dipping nature of the North Qilian fault along the top of a high-resistivity body beneath the NQLS, as indicated by an electrical structure (Xiao et al., 2012), points toward underthrusting as the principal factor, contributing to the complex crustal structure in the northern Tibetan Plateau.

The distributed shortening model has also played a role in the crustal deformation of the northern Tibetan Plateau, as indicated by the presence of D1 in our seismic imaging. A recent deep seismic reflection profile also provided evidence for decoupled crustal deformation (Huang et al., 2021), aligning with our observations (Figure 8). Thrust faults are prevalent in NQLS, extending northward into HXBS (Zheng et al., 2013; Zuza et al., 2018; Xiong et al., 2019). Surface active fault surveys unveiled north-directed overthrusting faults that traverse through HXBS and enter the Beishan Block (Zheng et al., 2021; Wang et al., 2022). Combining our seismic imaging with earthquake distribution, we deduced that the primary mechanism accommodating upper crust deformation involves folding and northward overthrusting. Notably, several near-flat, arc-shaped positive amplitudes above the Moho suggest that duplexing plays a crucial role in lower crustal shortening. This is supported by prominent reflections recorded in deep seismic profiles (Huang et al., 2021).

Our investigation unearthed a Moho ramp within the Jiuquan Basin. Seismic phases indicate that M2 gradually deepens to approximately 50 km beneath the Huahai Basin but abruptly descends to 60 km below the Jiuquan Basin (Figure 8). Although most studies suggest gradual Moho deepening in this region, wide-angle reflection/refraction data confirm this trend (Gao et al., 2001; Huang et al., 2021; Ye et al., 2021). The concept of a lithospheric ramp, introduced by Zuza et al. (2018), posits that both underthrusting and crustal shortening have been continuously occurring since the Miocene on the same lithospheric ramp. The disrupted stair-like Moho features beneath the Jiuquan Basin, gradually deepening toward the southwest, closely resemble the lithospheric ramp model (Vergne et al., 2002; Zhou and Murphy, 2005; Hazarika et al., 2017; Lu et al., 2019; Tan et al., 2019). We contend that compressive stress generated by the Moho underthrusting ramp propagates from the Jiuquan Basin to NQLS and HXBS to the south, thereby inducing crustal deformation above this ramp. The Moho ramp model we propose strongly supports the crustal compression model in the Qilian Shan Block–Huahai Basin region (Figure 9).

6 Conclusion

Drawing on our receiver function image and the analysis presented previously, we have outlined a comprehensive tectonic representation on a crustal scale that encapsulates our observations and interpretations beneath the North Qilian–Huahai Basin (Figure 9). By amalgamating our seismic imaging with additional geological and geophysical data, we propose the existence of a potential decoupling plane situated at a depth of 12–20 km. Within this framework, south-dipping brittle thrust faults govern upper crustal deformation, while imbricate structures and duplexes operate in the lower crust. Notably, we conjecture that the underthrusting of the Beishan Block beneath NQLS might be accountable for the occurrence of a double Moho. In addition, we posit that a Moho ramp could be developing beneath the Jiuquan Basin to accommodate the pronounced compression. In the western stretch of NQLS and HXBS, we propose that coupled distributed shortening and the underthrusting of the Beishan Block beneath the Qilian Shan fold-thrust belt might collaboratively contribute to the intricate crustal deformation.

Data availability statement

The original contributions presented in the study are included in the article/Supplementary Material; further inquiries can be directed to the corresponding author.

Author contributions

ZW: data curation, formal analysis, methodology, visualization, and writing–original draft. XX: conceptualization, funding acquisition, investigation, methodology, project administration,

supervision, writing–original draft, and writing–review and editing. GW: data curation, investigation, methodology, visualization, and writing–original draft. ZL: investigation, visualization, and writing–original draft. ZY: formal analysis, software, and writing–original draft. ZJ: formal analysis, software, and writing–original draft.

Funding

This study was funded by the National Natural Science Foundation of China (42274134, 41774114, and 42261144669) and the China Geological Survey Project (Grant Nos DD20230229 and DD20179342).

Conflict of interest

The authors declare that the research was conducted in the absence of any commercial or financial relationships that could be construed as a potential conflict of interest.

Publisher's note

References

Ammon, C. J., Randall, G. E., and Zandt, G. (1990). On the Nonuniqueness of Receiver function inversions. *J. Geophys. Res. Solid Earth* 95 (B10), 15303–15318. doi:10.1029/JB095iB10p15303

Bird, P. (1991). Lateral extrusion of lower crust from under high topography in the isostatic limit. *J. Geophys. Res. Solid Earth* 96 (B6), 10275–10286. doi:10.1029/91JB00370

Burke, K., and Dewey, J. F. (1973). Plume-generated triple junctions: key indicators in applying plate tectonics to old rocks. *J. Geol.* 81 (4), 406–433. doi:10.1086/627882

Chen, Q., Yang, Z., Zhu, M., Lin, X. f., and Xie, Z. l. (2010). Petroleum geology of Pan-Hexi Corridor basins and exploration prospecting. *Nat. Gas. Geosci.* 21 (2), 186–189. In Chinese. doi:10.3760/cma.j.issn.1003-9406.2010.02.015

Chen, L., Wang, X., Wang, X., Wei, Z. G., and Zhang, J. Y. (2022). Advances and perspectives for receiver function imaging of the Earth's internal discontinuities and velocity structures. *Rev. Geophys. Planet. Phys.* 53 (6), 680–701. doi:10.19975/j.dqyxx.2022-029

Cheng, F., Garzione, C. N., Mitra, G., Jolivet, M., Guo, Z., Lu, H., et al. (2019). The interplay between climate and tectonics during the upward and outward growth of the Qilian Shan orogenic wedge, northern Tibetan Plateau. *Earth-Science Rev.* 198, 102945. doi:10.1016/j.earscirev.2019.102945

Cheng, Y., Gao, R., Chen, J., Lu, Z., Li, W., Wang, G., et al. (2023). Crustal structure and geodynamics of the eastern Qilian orogenic belt, NE margin of the Qinghai-Tibet plateau, revealed by teleseismic receiver function. *Front. Earth Sci.* 11, 1193167. doi:10.3389/feart.2023.1193167

Clark, M. K., and Royden, L. H. (2000). Topographic ooze: building the eastern margin of Tibet by lower crustal flow. *Geology* 28 (8), 703–706. doi:10.1130/0091-7613(2000)028<0703:tobtem>2.3.co;2

Craddock, W., Kirby, E., and Zhang, H. (2011). Late Miocene–Pliocene range growth in the interior of the northeastern Tibetan Plateau. *Lithosphere* 3 (6), 420–438. doi:10.1130/L159.1

Craddock, W. H., Kirby, E., Zhang, H., Clark, M. K., Champagnac, J.-D., and Yuan, D. (2014). Rates and style of cenozoic deformation around the gonghe basin, northeastern Tibetan plateau. *Geosphere* 10 (6), 1255–1282. doi:10.1130/GES01024.1

Cui, Z. Z., Li, Q. S., Wu, C. D., and Liu, H. (1995). The crustal and deep structures in Golmud-Ejin Qi GGT (in Chinese with English abstract). *J. Geophys.* (S2), 15–28. http://geophy.cn/article/id/cjg_7335.

Dewey, J. F., Shackleton, R. M., Chengfa, C., Yiyin, S., Chengfa, C., Shackleton, R. M., et al. (1997). The tectonic evolution of the Tibetan Plateau. *Philosophical Trans. R. Soc. Lond. Ser. A, Math. Phys. Sci.* 327 (1594), 379–413. doi:10.1098/rsta.1988.0135

Dueker, K. G., and Sheehan, A. F. (1997). Mantle discontinuity structure from midpoint stacks of converted P to S waves across the Yellowstone hotspot track. *J. Geophys. Res. Solid Earth* 102, 8313–8327. doi:10.1029/96JB03857

Duvall, A. R., Clark, M. K., Kirby, E., Farley, K. A., Craddock, W. H., Li, C., et al. (2013). Low-temperature thermochronometry along the Kunlun and haiyuan faults, NE Tibetan plateau: evidence for kinematic change during late-stage orogenesis: TIMING of STRIKE-SLIP faulting tibet. *Tectonics* 32 (5), 1190–1211. doi:10.1002/tect.20072

England, P., and Houseman, G. (1986). Finite strain calculations of continental deformation: 2. Comparison with the India-Asia Collision Zone. *J. Geophys. Res. Solid Earth* 91 (B3), 3664–3676. doi:10.1029/JB091iB03p03664

Feng, M., Kumar, P., Mechie, J., Zhao, W., Kind, R., Su, H., et al. (2014). Structure of the crust and mantle down to 700 km depth beneath the East Qaidam basin and Qilian Shan from P and S receiver functions. *Geophys. J. Int.* 199 (3), 1416–1429. doi:10.1093/gji/ggu335

Gao, R., Cheng, X. Z., and Wu, G. J. (1999). "Lithospheric structure and geodynamic model of the Golmud-Ejin transect in northern Tibetan plateau," in *Himalaya and Tibet: mountain roots to mountain tops*. Editors A. Macfarlane, R. B. Sorkhabi, and J. Quade (Geological Society of America), 328, 0. doi:10.1130/0-8137-2328-0.9

Gao, R., Li, P. W., Li, Q. S., Guan, Y., Shi, D. N., Kong, X. R., et al. (2001). Deep process of the collision and deformation on the northern margin of the Tibetan Plateau: revelation from investigation of the deep seismic profiles. *Sci. China Ser. D.* 44, 71–78. doi:10.1007/BF02911973

Gao, R., Wang, H., Yin, A., Dong, S., Kuang, Z., Zuza, A. V., et al. (2013). Tectonic development of the northeastern Tibetan Plateau as constrained by high-resolution deep seismic-reflection data. *Lithosphere* 5, 555–574. doi:10.1130/L293.1

Hazarika, D., Wadhawan, M., Paul, A., Kumar, N., and Borah, K. (2017). Geometry of the main himalayan thrust and Moho beneath satluj valley, northwest himalaya: constraints from receiver function analysis. *J. Geophys. Res. Solid Earth* 122 (4), 2929–2945. doi:10.1002/2016JB013783

He, C. (2020). Upwelling mantle plume and lithospheric delamination beneath the North China Craton. *Phys. Earth Planet. Interiors* 306, 106548. doi:10.1016/j.pepi.2020.106548

Huang, X. F., Gao, R., Guo, X. Y., Li, W. H., and Xiong, X. S. (2018). Deep crustal structure beneath the junction of the Qilian Shan and Jiuxi Basin in the northeastern margin of the Tibetan Plateau and its tectonic implications. *Chin. J. Geophys* 61 (9), 3640–3650. (in Chinese). doi:10.6038/cig2018L0632

Huang, X., Gao, R., Li, W., and Xiong, X. (2021). Seismic reflection evidence of crustal duplexing and lithospheric underthrusting beneath the western Qilian Mountains, northeastern margin of the Tibetan Plateau. *Sci. China Earth Sci.* 64, 96–109. doi:10.1007/s11430-020-9677-y

Ingalls, M. L., and Stedman, R. C. (2016). The power problematic exploring the uncertain terrains of political ecology and the resilience framework. *Ecol. Soc.* 21 (1), art6. doi:10.5751/ES-08124-210106

Jolivet, M., Brunel, M., Seward, D., Xu, Z., Yang, J., Roger, F., et al. (2001). Mesozoic and Cenozoic tectonics of the northern edge of the Tibetan plateau: fission-track constraints. *Tectonophysics* 343 (1), 111–134. doi:10.1016/S0040-1951(01)00196-2

Kao, H., Gao, R., Rau, R. J., Shi, D. N., Chen, R. Y., Guan, Y., et al. (2001). Seismic image of the Tarim basin and its collision with Tibet. *Geology* 29, 575–578. doi:10.1130/0091-7613(2001)029<0575:SIOTTB>2.0.CO;2

Kennett, B. L. N., and Saygin, E. (2015). The nature of the Moho in Australia from reflection profiling: a review. *GeoResJ* 5, 74–91. doi:10.1016/j.grj.2015.02.001

Kind, R., Yuan, X., Saul, J., Nelson, D., Sobolev, S., Mechie, J., et al. (2002). Seismic images of crust and upper mantle beneath Tibet: evidence for Eurasian plate subduction. *science* 298 (5596), 1219–1221. doi:10.1126/science.1078115

Langston, C. A. (1979). Structure under Mount Rainier, Washington, inferred from teleseismic body waves. *J. Geophys. Res.* 84 (B9), 4749–4762. doi:10.1029/JB084iB09p04749

Lease, R. O., Burbank, D. W., Hough, B., Wang, Z., and Yuan, D. (2012). Pulsed Miocene range growth in northeastern Tibet: insights from Xunhua Basin magneto stratigraphy and provenance. *GSA Bull.* 124 (5-6), 657–677. doi:10.1130/B30524.1

Ligorria, J. P., and Ammon, C. J. (1999). Iterative deconvolution and receiver function estimation[J]. *Bulletin of the seismological Society of America* 89 (5), 1395–1400. doi:10.1785/BSSA0890051395

Lin, X., Chen, H., Wyrwoll, K.-H., Batt, G. E., Liao, L., and Xiao, J. (2011). The uplift history of the haiyuan-liupan Shan region northeast of the present Tibetan plateau: integrated constraint from stratigraphy and thermochronology. *J. Geol.* 119 (4), 372–393. doi:10.1086/660190

Liu, M., Mooney, W. D., Li, S., Okaya, N., and Detweiler, S. (2006). Crustal structure of the north eastern margin of the Tibetan Plateau from the Songpan-Ganzi terrane to the Ordos basin. *Tectonophysics* 420 (1–2), 253–266. doi:10.1016/j.tecto.2006.01.025

Lu, R., Liu, Y., Xu, X., Tan, X., He, D., Yu, G., et al. (2019). Three-Dimensional model of the lithospheric structure under the eastern Tibetan plateau: implications for the active tectonics and seismic hazards. *Tectonics* 38 (4), 1292–1307. doi:10.1029/2018TC005239

Molnar, P., and Tapponnier, P. (1975). Cenozoic Tectonics of Asia: effects of a Continental Collision: features of recent continental tectonics in Asia can be interpreted as results of the India-Eurasia collision. *science* 189 (4201), 419–426. doi:10.1126/science.189.4201.419

Molnar, P. (1988). Continental tectonics in the aftermath of plate tectonics. *Nature* 335 (6186), 131–137. doi:10.1038/335131a0

Royden, L. H., Burchfiel, B. C., King, R. W., Wang, E., Chen, Z., Shen, F., et al. (1997). Surface deformation and lower crustal flow in eastern Tibet. *science* 276 (5313), 788–790. doi:10.1126/science.276.5313.788

Song, C. H., Fang, X. M., Li, J. J., Gao, J. P., Zhao, Z. J., and Fan, M. J. (2001). Sedimentary evolution and tectonic uplift of jiuxi basin in the northern margin of qinghai Tibetan plateau since 13 Ma. *China Sci. (Part D Earth Sci.* (S1), 155–162. doi:10.3321/j.issn:0023-074X.2001.14.017

Shen, X., Li, Y., Gao, R., Chen, X., Liu, M., Yuan, X., et al. (2020). Lateral growth of NE Tibetan Plateau restricted by the Asian lithosphere: Results from a dense seismic profile. *Gondwana Research* 87, 238–247. doi:10.1016/j.gr.2020.06.018

Sun, Q., Pei, S., Cui, Z., Chen, Y. J., Liu, Y., Xue, X., et al. (2021). A new growth model of the northeastern Tibetan Plateau from high-resolution seismic imaging by improved double-difference tomography. *Tectonophysics* 798, 228699. doi:10.1016/j.tecto.2020.228699

Tan, X., Liu, Y., Lee, Y.-H., Lu, R., Xu, X., Suppe, J., et al. (2019). Parallelism between the maximum exhumation belt and the Moho ramp along the eastern Tibetan Plateau margin: coincidence or consequence? *Earth Planet. Sci. Lett.* 507, 73–84. doi:10.1016/j.epsl.2018.12.001

Tapponnier, P., Zhi, Q. X., Roger, F., Meyer, B., Arnaud, N., Wittlinger, G., et al. (2001). Oblique stepwise rise and growth of the Tibet plateau. *science* 294 (5547), 1671–1677. doi:10.1126/science.105978

Tian, X., Bai, Z., Klemperer, S. L., Liang, X., Liu, Z., Wang, X., et al. (2021). Crustal-scale wedge tectonics at the narrow boundary between the Tibetan Plateau and Ordos block. *Earth Planet. Sci. Lett.* 554, 116700. doi:10.1016/j.epsl.2020.116700

van Hinsbergen, D. J. J., Kapp, P., Dupont-Nivet, G., Lippert, P. C., DeCelles, P. G., and Torsvik, T. H. (2011). Restoration of cenozoic deformation in asia and the size of greater India. *Tectonics* 30 (5). doi:10.1029/2011TC002908

van Hinsbergen, D. J. J., Lippert, P. C., Dupont-Nivet, G., McQuarrie, N., Doubrovine, P. V., Spakman, W., et al. (2012). Greater India Basin hypothesis and a two-stage cenozoic collision between India and asia. *Proc. Natl. Acad. Sci.* 109 (20), 7659–7664. doi:10.1073/pnas.1117262109

Vergne, J., Wittlinger, G., Hui, Q., Tapponnier, P., Poupinet, G., Mei, J., et al. (2002). Seismic evidence for stepwise thickening of the crust across the NE Tibetan plateau. *Earth Planet. Sci. Lett.* 203 (1), 25–33. doi:10.1016/s0012-821x(02)00853-1

Wang, W. T., Zhang, P. Z., Duan, L., Zhang, B. X., Liu, K., Huang, R., et al. (2022). Cenozoic stratigraphic chronology and sedimentary-tectonic evolution of the Qaidam Basin. *Chin. Sci. BULLETIN-CHINESE* 67 (28-29), 3452–3475. doi:10.1360/TB-2022-0108

Willett, S. D., and Beaumont, C. (1994). Subduction of Asian lithospheric mantle beneath Tibet inferred from models of continental collision. *Nature* 369 (6482), 642–645. doi:10.1038/369642a0

Wu, X. Z., Wu, C. L., Lu, J., and Wu, J. (1995). Research on the fine crustal structure of the Northerh Qilian-Nexi Corrior by deep seismic reflection. *Chinese Journal of Geophysics* 1995 (S2), 29–35.

Wu, C., Chen, X. H., and Ding, L. (2023a). Tectonic evolution and Cenozoic deformation history of the Qilian Shanic belt. *Geosci. Front.* 30 (03), 262–281. doi:10.13745/j.esf.sf.2022.12.20

Wu, G. W., Xiong, X. S., Gao, R., Chen, X. H., Li, Y. K., Wang, J., et al. (2023b). Moho depth of the Qilian Shan revealed by wide-angle reflection/refraction profiles. *Rev. Geophys. Planet. Phys.* 54 (2), 109–119. (in Chinese). doi:10.19975/j.dqyxx.2021-067

Xiao, Q., Zhang, J., Wang, J., Zhao, G., and Tang, J. (2012). Electrical resistivity structures between the northern qilian mountains and beishan block, NW China, and tectonic implications. *Phys. Earth Planet. Interiors* 200-201, 92–104. doi:10.1016/j.pepi.2012.04.008

Xiong, X. S., Gao, R., Feng, S. Y., Li, Y. K., Huang, X. F., Chen, X. H., et al. (2019). Deep structure of Yumushan tectonic zone and genesis of the uplift. *Geol. China* 46 (5), 1039–1051. (in Chinese with English abstract). doi:10.12029/gc20190506

Xiong, X., Wang, G., Li, Q., Lu, Z., Gao, R., Feng, S., et al. (2022). Crustal structure of the chuan-dian block revealed by deep seismic sounding and its implications for the outward expansion of the east Tibetan plateau. *Acta Geol. Sin. - Engl. Ed.* 96 (6), 1932–1944. doi:10.1111/1755-6724.14922

Xu, X., Niu, F., Ding, Z., and Chen, Q. (2018). Complicated crustal deformation beneath the NE margin of the Tibetan plateau and its adjacent areas revealed by multi station receiver-function gathering. *Earth Planet. Sci. Lett.* 497, 204–216. doi:10.1016/j.epsl.2018.06.010

Xu, Q., Pei, S., Yuan, X., Zhao, J., Liu, H., Tu, H., et al. (2019). Seismic evidence for lateral asthenospheric flow beneath the northeastern Tibetan Plateau derived from S receiver functions. *Geochem. Geophys. Geosyst.* 20 (2), 883–894. doi:10.1029/2018GC007986

Xu, M., Huang, Z., Wang, L., Xu, M., Zhang, Y., Mi, N., et al. (2020). Sharp lateral Moho variations across the SE Tibetan margin and their implications for plateau growth. *J. Geophys. Res. Solid Earth* 125 (5), e2019JB018117. doi:10.1029/2019JB018117

Yakovlev, P. V., and Clark, M. K. (2014). Conservation and redistribution of crust during the Indo-Asian collision. *Tectonics* 33 (6), 1016–1027. doi:10.1002/2013TC003469

Yang, S. F., Chen, H. L., Cheng, X. G., Xiao, A. C., He, G. Y., and Chen, J. J. (2007). Deformation characteristics and rules of spatial change for the northern qilianshan thrust belt. *Earth Sci. Front.* 14 (5), 211–221. doi:10.1016/S1872-5791(08)60012-3

Ye, Z., Gao, R., Li, Q., Zhang, H., Shen, X., Liu, X., et al. (2015). Seismic evidence for the North China plate underthrusting beneath northeastern Tibet and its implications for plateau growth. *Earth Planet. Sci. Lett.* 426, 109–117. doi:10.1016/j.epsl.2015.06.024

Ye, Z., Gao, R., Lu, Z., Yang, Z., Xiong, X., Li, W., et al. (2021). A lithospheric-scale thrust-wedge model for the formation of the northern Tibetan plateau margin:Evidence from high-resolution seismic imaging. *Earth Planet. Sci. Lett.* 574, 117170. doi:10.1016/j.epsl.2021.117170

Yin, A., and Harrison, T. M. (2000). Geologic evolution of the Himalayan-Tibetan orogen. *Annu. Rev. earth Planet. Sci.* 28 (1), 211–280. doi:10.1146/annurev.earth.28.1.211

Yin, A., Rumelhart, P. E., Butler, R., Cowgill, E., Harrison, T. M., Foster, D. A., et al. (2002). Tectonic history of the Altyn Tagh fault system in northern Tibet inferred from Cenozoic sedimentation. *GSA Bull.* 114 (10), 1257–1295. doi:10.1130/0016-7606(2002)114<1257:THOTAT>2.0.CO;2

Yin, A. (2000). Mode of Cenozoic east-west extension in Tibet suggesting a common origin of rifts in Asia during the Indo-Asian collision. *J. Geophys. Res. Solid Earth* 105 (B9), 21745–21759. doi:10.1029/2000JB900168

Yin, A. (2010). Cenozoic tectonic evolution of Asia:A preliminary synthesis. *Tectonophysics* 488 (1), 293–325. doi:10.1016/j.tecto.2009.06.002

Yuan, D.-Y., Ge, W.-P., Chen, Z.-W., Li, C.-Y., Wang, Z.-C., Zhang, H.-P., et al. (2013). The growth of northeastern Tibet and its relevance to large-scale continental geodynamics: a review of recent studies. *Tectonics* 32 (5), 1358–1370. doi:10.1002/tect.20081

Yue, H., Chen, Y. J., Sandvol, E., Ni, J., Hearn, T., Zhou, S., et al. (2012). Lithospheric and upper man-tle structure of the northeastern Tibetan Plateau. *J. Geophys. Res.* 117, B05307. doi:10.1029/2011JB008545

Zhang, Z. J., Qin, Y. L., Chen, Y., Zhang, C. Y., Sun, S. X., Zhao, B., et al. (2004). Reconstruction of semblance section for the crust/mantle reflection structure by wide-angle seismic data. *Chin. J. Geophys.* 47 (3), 533–538. doi:10.1002/cjg2.517

Zhao, W.-L., and Morgan, W. J. (1987). Injection of Indian crust into Tibetan lower crust: a two-dimensional finite element model study. *Tectonics* 6 (4), 489–504. doi:10.1029/TC006i004p00489

Zhao, W., Nelson, K. D., Che, J., Quo, J., Lu, D., Wu, C., et al. (1993). Deep seismic reflection evidence for continental underthrusting beneath southern Tibet. *Nature* 366 (6455), 557–559. doi:10.1038/366557a0

Zhao, G., Wilde, S. A., Cawood, P. A., and Sun, M. (2001). Archean blocks and their boundaries in the North China Craton: lithological, geochemical, structural and P–T path constraints and tectonic evolution. *Precambrian Res.* 107 (1), 45–73. doi:10.1016/S0301-9268(00)00154-6

Zhao, J., Yuan, X., Liu, H., Kumar, P., Pei, S., Kind, R., et al. (2010). The boundary between the Indian and Asian tectonic plates below Tibet. *Proc. Natl. Acad. Sci. U. S. A.* 107, 11229–11233. doi:10.1073/pnas.1001921107

Zhao, D., Huang, Z., Umino, N., Hasegawa, A., and Kanamori, H. (2011). Structural heterogeneity in the megathrust zone and mechanism of the 2011 Tohoku-oki earthquake (Mw 9.0). *Geophys. Res. Lett.* 38 (17). doi:10.1029/2011GL048408

Zheng, W. J., Zhang, P. Z., Ge, W. P., Molnar, P., Zhang, H. P., Yuan, D. Y., et al. (2013). Late quaternary slip rate of the south heli Shan fault (northern Hexi corridor, NW China) and its implications for northeastward growth of the Tibetan plateau. *Tectonics* 32, 271–293. doi:10.1002/tect.20022

Zheng, D., Wang, W., Wan, J., Yuan, D., Liu, C., Zheng, W., et al. (2017). Progressive northward growth of the northern qilian Shan–Hexi corridor (northeastern Tibet) during the cenozoic. *Lithosphere* 9 (3), 408–416. doi:10.1130/L587.1

Zheng, W., Bi, H., Wang, X., Zhang, D., Huang, R., Zhang, P., et al. (2021). Constraining paleoearthquakes by combining faulted stratigraphy and microgeomorphology: a case study on the haiyuan fault, northwestern China. *Seismol. Res. Lett.* 92 (2A), 895–908. doi:10.1785/0220200143

Zhou, H. W., and Murphy, M. A. (2005). Tomographic evidence for wholesale underthrusting of India beneath the entire Tibetan Plateau. *Journal of Asian Earth Sciences* 25 (3), 445–457. doi:10.1016/j.jseaes.2004.04.007

Zhou, D., Wang, W., Wang, J., Pang, X., Cai, D., and Sun, Z. (2006). Mesozoic subduction-accretion zone in northeastern south China sea inferred from geophysical interpretations. *Sci. China Ser. D* 49 (5), 471–482. doi:10.1007/s11430-006-0471-9

Zhu, L. P., and Kanamori, H. (2000). Moho depth variation in southern California from teleseismic receiver functions. *J. Geophys. Res.* 105, 2969–2980. doi:10.1029/1999JB900322

Zuza, A. V., Cheng, X., and Yin, A. (2016). Testing models of Tibetan Plateau formation with Cenozoic shortening estimates across the Qilian Shan–Nan Shan thrust belt. *Geosphere* 12 (2), 501–532. doi:10.1130/GES01254.1

Zuza, A. V., Wu, C., Reith, R. C., Yin, A., Li, J., Zhang, J., et al. (2018). Tectonic evolution of the Qilian Shan: an early Paleozoic orogen reactivated in the Cenozoic. *Geol. Soc. Am. Bull.* 130, 881–925. doi:10.1130/b31721.1

Zuza, A. V., Wu, C., Wang, Z., Levy, D. A., Li, B., Xiong, X., et al. (2019). Underthrusting and duplexing beneath the northern Tibetan Plateau and the evolution of the Himalayan-Tibetan orogen. *Lithosphere* 11 (2), 209–231. doi:10.1130/L1042.1